B MARTIN
Nuclear and Particle Physics
(Wiley, 2006)
Chapter 02 - Nuclear physics

2

Nuclear Phenomenology

In this chapter we start to examine some of the things that can be learned from experiments, beginning with basic facts about nuclei, including what can be deduced about their shapes and sizes. Then we discuss the important topic of nuclear stability and the phenomenology of the various ways that unstable nuclei decay to stable states. Finally, we briefly review the classification of reactions in nuclear physics. Before that we need to introduce some notation.

2.1 Mass Spectroscopy and Binding Energies

Nuclei are specified by:

Z – atomic number = the number of protons,

N – neutron number = the number of neutrons,

A – mass number = the number of nucleons, so that $A = Z + N$.

We will also refer to A as the *nucleon number*. The charge on the nucleus is $+Ze$, where e is the absolute value of the electric charge on the electron. Nuclei with combinations of these three numbers are also called *nuclides* and are written ${}^{A}\mathrm{Y}$ or ${}^{A}_{Z}\mathrm{Y}$, where Y is the chemical symbol for the element. Some other common nomenclature is:

nuclides with the same mass number are called *isobars*,

nuclides with the same atomic number are called *isotopes*,

nuclides with the same neutron number are called *isotones*.

Nuclear and Particle Physics B. R. Martin
 ISBN: 0-470-01999-9

The concept of isotopes was introduced in Chapter 1. For example, stable isotopes of carbon are ^{12}C and ^{13}C, and the unstable isotope used in dating ancient objects (see later in this chapter) is ^{14}C; all three have $Z = 6$.

Just as in the case of electrons in atoms, the forces that bind the nucleons in nuclei contribute to the total mass of an atom $M(Z, A)$ and in terms of the masses of the proton M_p and neutron M_n

$$M(Z,A) < Z\,(M_p + m_e) + N\,M_n. \tag{2.1}$$

The *mass deficit* is defined as

$$\Delta M(Z,A) \equiv M(Z,A) - Z\,(M_p + m_e) - N\,M_n \tag{2.2}$$

and $-\Delta Mc^2$ is called the *binding energy B*. Binding energies may be calculated if masses are measured accurately. One way of doing this is by using the techniques of *mass spectroscopy*. The principle of the method is shown in Figure 2.1.

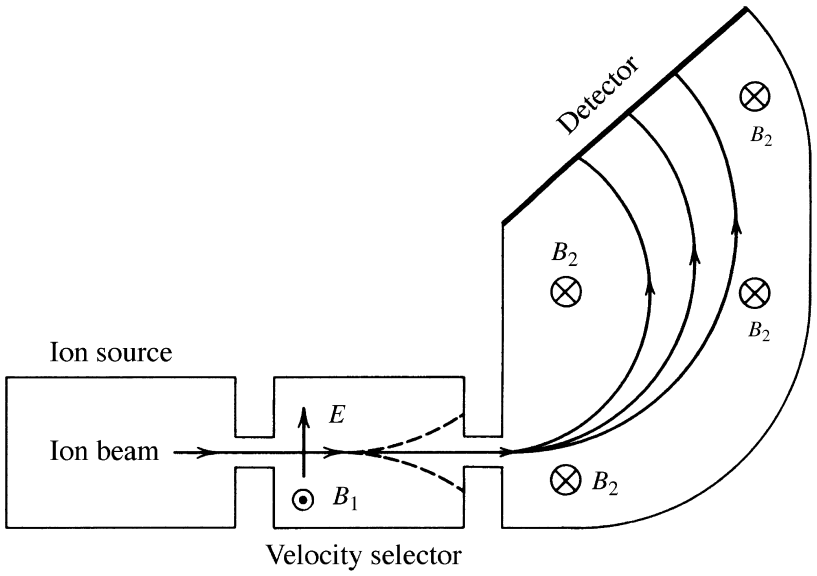

Figure 2.1 Schematic diagram of a mass spectrometer (adapted from Kr88 Copyright John Wiley & Sons, Inc.)

A source of ions of charge q, containing various isotopes passes through a region where there are uniform electric (E) and magnetic (B_1) fields at right angles. The electric field will exert a force qE in one direction and the magnetic field will exert a force qvB_1 in the opposite direction, where v is the speed of the ions. By balancing these forces, ions of a specific speed $v = E/B_1$ can be selected and allowed to pass through a collimating slit. Ions with other velocities (shown as dashed lines) are deflected. The beam is then allowed to continue through a second

uniform magnetic field B_2 where it will be bent into a circular path of radius ρ, given by

$$mv = qB_2\rho \tag{2.3}$$

and since q, B_2 and v are fixed, particles with a fixed ratio q/m will bend in a path with a unique radius. Hence isotopes may be separated and focused onto a detector (e.g. a photographic plate). In the common case where $B_1 = B_2 = B$,

$$\frac{q}{m} = \frac{E}{B^2\rho}. \tag{2.4}$$

In practice, to achieve high accuracy, the device is used to measure mass differences rather than absolute values of mass.[1]

Conventional mass spectroscopy cannot be used to find the masses of very short-lived nuclei and in these cases the masses are determined from kinematic analysis of nuclear reactions as follows. Consider the inelastic reaction $A(a,a)A^*$, where A^* is the short-lived nucleus whose mass is to be determined. The kinematics of this are:

$$a(E_i, \mathbf{p}_i) + A(m_Ac^2, \mathbf{0}) \rightarrow a(E_f, \mathbf{p}_f) + A^*(\tilde{E}, \tilde{\mathbf{p}}), \tag{2.5}$$

where we use tilded quantities to denote the energy, mass, etc. of A^*. Equating the total energy before the collision

$$E_{\text{tot}}(\text{initial}) = E_i + m_ac^2 + m_Ac^2 \tag{2.6a}$$

to the total energy after the collision

$$E_{\text{tot}}(\text{final}) = E_f + \tilde{E} + m_ac^2 + \tilde{m}\,c^2 \tag{2.6b}$$

gives the following expression for the change in energy of the nucleus:

$$\Delta E \equiv (\tilde{m} - m_A)c^2 = E_i - E_f - \tilde{E} = \frac{p_i^2}{2m_a} - \frac{p_f^2}{2m_a} - \frac{\tilde{p}^2}{2\tilde{m}}, \tag{2.7}$$

where we have assumed non-relativistic kinematics. If the initial momentum of the projectile is along the x-direction and the scattering angle is θ, then from momentum conservation,

$$(\tilde{p})_x = p_i - p_f\cos\theta\,, \qquad (\tilde{p})_y = p_f\sin\theta \tag{2.8}$$

[1]Practical details of mass spectroscopy may be found in, for example, Chapter 3 of Kr88.

and using these in Equation (2.7) gives

$$\Delta E = E_i\left(1 - \frac{m_a}{\tilde{m}}\right) - E_f\left(1 + \frac{m_a}{\tilde{m}}\right) + \frac{2m_a}{\tilde{m}}\left(E_i E_f\right)^{1/2}\cos\theta. \tag{2.9}$$

This formula can be used iteratively to deduce ΔE and hence the mass of the excited nucleus A^*, from measurements of the initial and final energy of the projectile by initially setting $\tilde{m} = m_A$ on the right-hand side because ΔE is small in comparison with m_A. One final point is that the energies in Equation (2.9) are measured in the laboratory system, whereas the final energies (masses) will be needed in the centre-of-mass system.[2] The necessary transformation is easily found to be

$$E_{\mathrm{CM}} = E_{\mathrm{lab}}(1 + m_a/m_A)^{-1}. \tag{2.10}$$

A similar formula to Equation (2.9) may be derived for the general reaction $A(a,b)B$:

$$\Delta E = E_i\left(1 - \frac{m_a}{m_B}\right) - E_f\left(1 + \frac{m_b}{m_B}\right) + \frac{2}{m_B}\left(m_a m_b E_i E_f\right)^{1/2}\cos\theta + Q, \tag{2.11}$$

where Q is the kinetic energy released in the reaction.

A commonly used quantity of interest is the *binding energy per nucleon* B/A. This is shown schematically in Figure 2.2 for nuclei that are stable or long-lived.

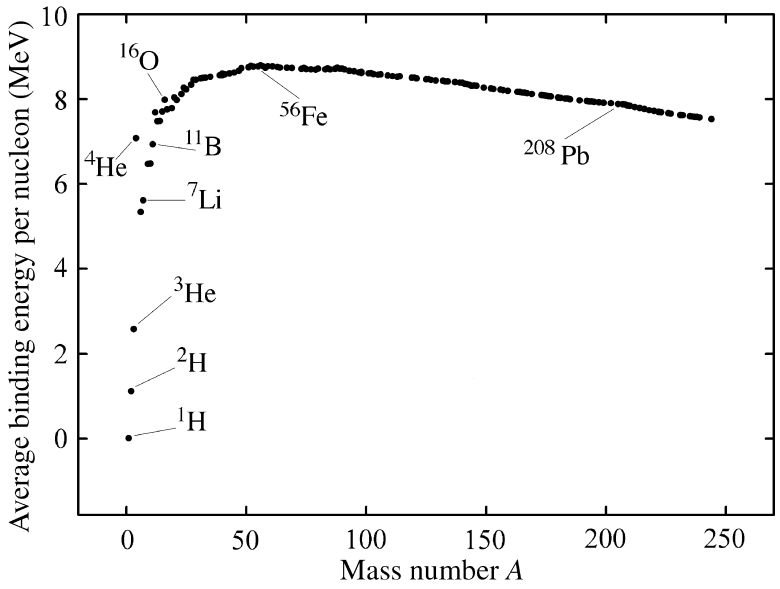

Figure 2.2 Binding energy per nucleon as a function of mass number A for stable and long-lived nuclei

[2] A discussion of these two systems is given in Appendix C.

This shows that B/A peaks at a value of 8.7 MeV for a mass number of about 56 (close to iron) and thereafter falls very slowly. Excluding very light nuclei, the binding energy per nucleon is between 7 and 9 MeV over a wide range of the periodic table. In Section 2.5 we will discuss a model that provides an explanation for the shape of this curve.

2.2 Nuclear Shapes and Sizes

The shape and size of a nucleus may be found from scattering experiments; i.e. a projectile is scattered from the nucleus and the angular distribution of the scattered particles examined, as was done by Rutherford and his collaborators when they deduced the existence of the nucleus. The interpretation is simplest in those cases where the projectile itself has no internal structure, i.e. it is an elementary particle, and electrons are often used. In this case the relevant force is electromagnetic and we learn about the *charge distribution* in the nucleus. The first experiments of this type were performed by Hofstader and his collaborators in the late 1950s.[3] If instead of an electron a hadron is used as the projectile, the force is dominantly the nuclear strong interaction and we find information about the *matter density*. Neutrons are commonly used so that Coulomb effects are absent. We discuss these two cases in turn.

2.2.1 Charge distribution

To find the amplitude for electron–nucleus scattering, we should in principle solve the Schrödinger (or Dirac) equation using a Hamiltonian that includes the full electromagnetic interaction and use nuclear wavefunctions. This can only be done numerically. However, in Appendix C we derive a simple formula that describes the electromagnetic scattering of a charged particle in the so-called *Born approximation*, which assumes $Z\alpha \ll 1$ and uses plane waves for the initial and final states. This leads to the *Rutherford cross-section*, which in its relativistic form may be written

$$\left(\frac{\mathrm{d}\sigma}{\mathrm{d}\Omega}\right)_{\text{Rutherford}} = \frac{Z^2\alpha^2(\hbar c)^2}{4E^2\sin^4(\theta/2)}, \tag{2.12}$$

where E is the total initial energy of the projectile and θ is the angle through which it is scattered. Note that Equation (2.12) is of order α^2 because it corresponds to the exchange of a single photon. Although Equation (2.12) has a limited range of applicability, it is useful to discuss the general features of electron scattering.

Equation (2.12) actually describes the scattering of a spin-0 point-like projectile of unit charge from a fixed point-like target with electric charge Ze, i.e. the charge

[3] Robert Hofstader shared the 1961 Nobel Prize in Physics for his pioneering electron scattering experiments.

distribution of the target is neglected. It therefore needs to be modified in a number of ways before it can be used in practice. We will state the modifications without proof.

Firstly, taking account of the electron spin leads to the so-called *Mott cross-section*

$$\left(\frac{\mathrm{d}\sigma}{\mathrm{d}\Omega}\right)_{\text{Mott}} = \left(\frac{\mathrm{d}\sigma}{\mathrm{d}\Omega}\right)_{\text{Rutherford}} \left[1 - \beta^2 \sin^2(\theta/2)\right], \tag{2.13}$$

where $\beta = v/c$ and v is the velocity of the initial electron. At higher energies, the recoil of the target needs to be taken into account and this introduces a factor E'/E on the right-hand side of Equation (2.13), where E' is the final energy of the electron. At higher energies we also need to take account of the interaction with the magnetic moment of the target in addition to its charge. The final form for the differential cross-section is

$$\left(\frac{\mathrm{d}\sigma}{\mathrm{d}\Omega}\right)_{\text{spin } \frac{1}{2}} = \left(\frac{\mathrm{d}\sigma}{\mathrm{d}\Omega}\right)_{\text{Mott}} \frac{E'}{E} \left[1 + 2\tau \tan^2 \frac{\theta}{2}\right], \tag{2.14}$$

where

$$\tau = \frac{-q^2}{4M^2c^2} \tag{2.15}$$

and M is the target mass. Because the energy loss of the electron to the recoiling nucleus is no longer negligible, $\mathbf{q}$, the previous momentum transfer, has been replaced by the four-momentum transfer q, whose square is

$$q^2 = (p - p')^2 = 2m_e^2c^2 - 2(EE'/c^2 - |\mathbf{p}||\mathbf{p}'|\cos\theta) \approx -\frac{4EE'}{c^2}\sin^2(\theta/2), \tag{2.16}$$

where $p(p')$ is the four-momentum of the initial (final) electron. (Because $q^2 \leq 0$, it is common practice to replace it with $Q^2 = -q^2$, so as to work with positive quantities.[4]) For the rest of this discussion it will be sufficient to ignore the magnetic interaction, although we will use a variant of the full form (2.16) in Chapter 6.

The final modification is due to the spatial extension of the nucleus. If the spatial charge distribution within the nucleus is written $f(\mathbf{x})$ then we define the *form factor* $F(\mathbf{q}^2)$ by

$$F(\mathbf{q}^2) \equiv \frac{1}{Ze}\int \mathrm{e}^{iq\cdot\mathbf{x}/\hbar} f(\mathbf{x})\,\mathrm{d}^3\mathbf{x} \quad \text{with} \quad Ze = \int f(\mathbf{x})\,\mathrm{d}^3\mathbf{x}, \tag{2.17}$$

[4]To remove any confusion, in the non-relativistic case, which we use in the rest of this chapter, q is interpreted to be $q = |\mathbf{q}| \geq 0$ where $\mathbf{q} \equiv \mathbf{p} - \mathbf{p}'$, as was used in Section 1.6.1. We will need the four-momentum definition of q in Chapter 6.

i.e. the Fourier transform of the charge distribution.[5] In the case of a spherically symmetric charge distribution, the angular integrations in Equations (2.17) may be done using spherical polar coordinates to give

$$F(\mathbf{q}^2) = \frac{4\pi\hbar}{Zeq}\int_0^\infty r\rho(r)\sin\left(\frac{qr}{\hbar}\right)\mathrm{d}r, \tag{2.18}$$

where $q = |\mathbf{q}|$ and $\rho(r)$ is the radial charge distribution. The final form of the experimental cross-section in this approximation is given by[6]

$$\left(\frac{\mathrm{d}\sigma}{\mathrm{d}\Omega}\right)_{\text{expt}} = \left(\frac{\mathrm{d}\sigma}{\mathrm{d}\Omega}\right)_{\text{Mott}} \left|F(\mathbf{q}^2)\right|^2. \tag{2.19}$$

Two examples of measured cross-sections are shown in Figure 2.3. Striking features are the presence of a number of well-defined minima superimposed on a

Figure 2.3 Elastic differential cross-sections as a function of the scattering angle for 450 MeV electrons from ^{58}Ni and 758 MeV electrons from ^{48}Ca; the solid lines are fits as described in the text (adapted from Si75 (^{58}Ni data) and Be67 (^{48}Ca data), Copyright American Physical Society)

[5]Strictly this formula assumes that the recoil of the target nucleus is negligible and the interaction is relatively weak, so that perturbation theory may be used.
[6]If the magnetic interaction were included, another form factor would be necessary, as is the case in high-energy electron scattering discussed in Chapter 6.

rapid decrease in the cross-section with angle. These features are common to all elastic data, although not all nuclei show so many minima as those shown.

The minima are due to the form factor and we can make this plausible by taking the simple case where the nuclear charge distribution is represented by a hard sphere such that

$$\begin{aligned} \rho(r) &= \text{constant}, \quad && r \leq a \\ &= 0 && r > a \end{aligned} \tag{2.20}$$

where a is a constant. In this case, evaluation of Equation (2.18) gives

$$F(\mathbf{q}^2) = 3[\sin(b) - b\cos(b)]b^{-3}, \tag{2.21}$$

where $b \equiv qa/\hbar$. Thus $F(\mathbf{q}^2)$ will be zero at values of b for which $b = \tan(b)$. In practice, as we will see below, $\rho(r)$ is not a hard sphere, and although it is approximately constant for much of the nuclear volume, it falls smoothly to zero at the surface. Smoothing the edges of the radial charge distribution (2.20) modifies the positions of the zeros, but does not alter the argument that the minima in the cross-sections are due to the spatial distribution of the nucleus. Their actual positions and depths result from a combination of the form factor and the form of the point-like amplitude. We shall see below that the minima can tell us about the size of the nucleus.

If one measures the cross-section for a fixed energy at various angles (and hence various q^2), the form factor can in principle be extracted using Equation (2.19) and one might attempt to find the charge distribution from the inverse Fourier transform

$$f(\mathbf{x}) = \frac{Ze}{(2\pi)^3} \int F(\mathbf{q}^2)\, \mathrm{e}^{-i\mathbf{q}\cdot\mathbf{x}/\hbar}\, \mathrm{d}^3\mathbf{q}. \tag{2.22}$$

However, $\mathbf{q}^2$ only has a finite range for a fixed initial electron energy and even within this range the rapid fall in the cross-section means that in practice measurements cannot be made over a sufficiently wide range of angles for the integral in Equation (2.22) to be evaluated accurately. Thus, even within the approximations used, reliable charge distributions cannot be found from Equation (2.22). Therefore different strategies must be used to deduce the charge distribution. In one approach, plausible – but very general – parameterized forms (for example a sum of Gaussians) are chosen for the charge distribution and are used to modify the point-like electromagnetic interaction. The resulting Schrödinger (or Dirac) equation is solved numerically to produce an amplitude, and hence a cross-section, for electron–nucleus scattering. The parameters of the charge distribution are then varied to give a good fit of the experimental data. The solid curves in Figure 2.3 are obtained in this way.

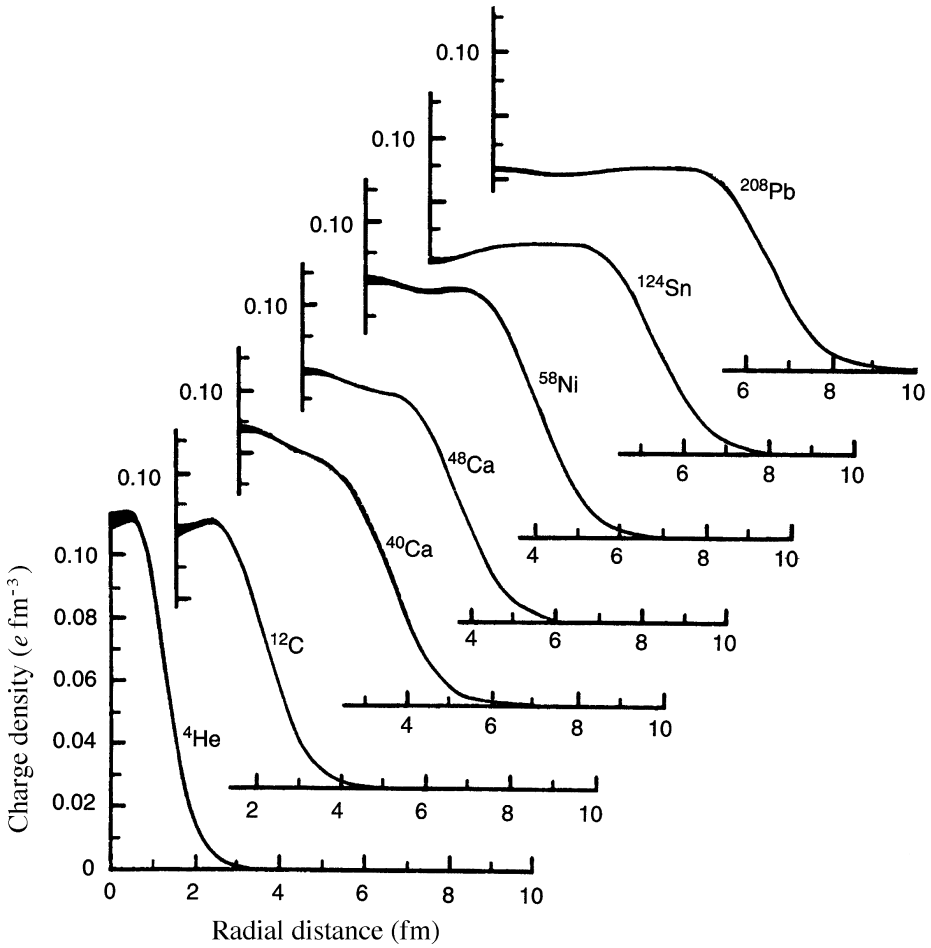

Figure 2.4 Radial charge distributions ρ_{ch} of various nuclei, in units of e fm^{-3}; the thickness of the curves near $r = 0$ is a measure of the uncertaintity in ρ_{ch} (adapted from Fr83)

Some radial charge distributions for various nuclei obtained by these methods are shown in Figure 2.4. They are well represented by the form

$$\rho_{\text{ch}}(r) = \frac{\rho_{\text{ch}}^0}{1 + \text{e}^{(r-a)/b}}, \tag{2.23}$$

where a and b for medium and heavy nuclei are found to be

$$a \approx 1.07A^{1/3}\ \text{fm} \quad \text{and} \quad b \approx 0.54\ \text{fm}. \tag{2.24}$$

From this we can deduce that the charge density is approximately constant in the nuclear interior and falls fairly rapidly to zero at the nuclear surface, as anticipated above. The value of ρ_{ch}^0 is in the range 0.06–0.08 for medium to heavy nuclei and decreases slowly with increasing mass number.

A useful quantity is the *mean square charge radius*,

$$\langle r^2 \rangle \equiv \int_0^\infty r^2 \rho_{\rm ch}(r)\, {\rm d}r. \tag{2.25}$$

This can be found from the form factor as follows. Expanding Equation (2.17) for $F(\mathbf{q}^2)$ gives

$$F(\mathbf{q}^2) = \frac{1}{Ze}\int f(\mathbf{x}) \sum_{n=0}^{\infty} \frac{1}{n!}\left(\frac{i|\mathbf{q}|r\cos\theta}{\hbar}\right)^n d^3\mathbf{x} \tag{2.26}$$

and after carrying out the angular integrations this becomes

$$F(\mathbf{q}^2) = \frac{4\pi}{Ze}\int_0^\infty f(r)\, r^2 dr - \frac{4\pi\mathbf{q}^2}{6Ze\hbar^2}\int_0^\infty f(r)\, r^4 dr + \ \cdots. \tag{2.27}$$

From the normalization of $f(\mathbf{x})$, we finally have

$$F(\mathbf{q}^2) = 1 - \frac{\mathbf{q}^2}{6\hbar^2}\langle r^2 \rangle + \ \cdots \tag{2.28}$$

and thus the mean square charge radius can be found from

$$\langle r^2 \rangle = -6\hbar^2 \frac{{\rm d}F(\mathbf{q}^2)}{{\rm d}\mathbf{q}^2}\bigg|_{\mathbf{q}^2=0}, \tag{2.29}$$

provided the form factor can be measured at very small values of $\mathbf{q}^2$. For medium and heavy nuclei $\langle r^2 \rangle^{1/2}$ is given approximately by[7]

$$\langle r^2 \rangle^{1/2} = 0.94 A^{1/3}\,{\rm fm}. \tag{2.30}$$

The nucleus is often approximated by a homogeneous charged sphere. The radius R of this sphere is then quoted as the nuclear radius. The relation of this to the mean square radius is $R^2 = \frac{5}{3}\langle r^2 \rangle$, so that

$$R_{\rm charge} = 1.21\, A^{1/3}\,{\rm fm}. \tag{2.31}$$

2.2.2 Matter distribution

Electrons cannot be used to obtain the distributions of neutrons in the nucleus. We could, however, take the presence of neutrons into account by multiplying $\rho_{\rm ch}(r)$

[7]The constant comes from a fit to a range of data, e.g. the compilation for $55 \leq A \leq 209$ given in Ba77.

by A/Z. Then we find an almost identical nuclear density in the nuclear interior for all nuclei, i.e. the decrease in ρ_{ch}^{0} with increasing A is compensated by the increase in A/Z with increasing A. The interior nuclear density is given by

$$\rho_{\mathrm{nucl}} \approx 0.17 \text{ nucleons/fm}^3. \tag{2.32}$$

Likewise, the effective nuclear matter radius for medium and heavy nuclei is

$$R_{\mathrm{nuclear}} \approx 1.2\,A^{1/3}\,\mathrm{fm}. \tag{2.33}$$

These are important results that will be used extensively later in this chapter and elsewhere in this book.

To probe the nuclear (i.e. matter) density of nuclei experimentally, a strongly interacting particle, i.e. a hadron, has to be used as the projectile. At high energies, where elastic scattering is only a small part of the total interaction, the nucleus behaves more like an absorbing sphere. In this case, the incident particle of momentum p will have an associated quantum mechanical wave of wavelength $\lambda = h/p$ and will suffer diffraction-like effects, as in optics. To the extent that we are dealing at high energies purely with the nuclear strong interaction (i.e. neglecting the Coulomb interaction), the nucleus can be represented by a black disk of radius R and the differential cross-section will have a Fraunhofer-like diffraction form, i.e.

$$\frac{\mathrm{d}\sigma}{\mathrm{d}\Omega} \propto \left[\frac{J_1(qR)}{qR}\right]^2, \tag{2.34}$$

where $qR \approx pR\theta$ for small θ and J_1 is a first-order Bessel function. For large qR,

$$[J_1(qR)]^2 \approx \left(\frac{2}{\pi qR}\right)\sin^2\left(qR - \frac{\pi}{4}\right), \tag{2.35}$$

which has zeros at intervals $\Delta\theta = \pi/pR$. The plausibility of this interpretation is borne out by experiment, an example of which is shown in Figure 2.5. The data show a succession of roughly equally spaced minima as suggested by Equation (2.35).

To go further requires solving the equations of motion, but this is far more problematical than in the electron case because the hadrons are more likely to be absorbed as they pass through the nucleus and the effective potential is far less well known. However, the analogy with optics can be pursued further in the so-called *optical model*. The essential idea in this model is that a hadron incident on a nucleus may be elastically scattered, or it may cause a variety of different reactions. As in the discussion above, if the incident particle is represented by a wave, then in classical language it may be scattered or it may be absorbed. In optics this is analogous to the refraction and absorption of a light wave by a medium of complex refractive index, and just as the imaginary part of the refractive index takes account of the absorption of the light wave, so in the

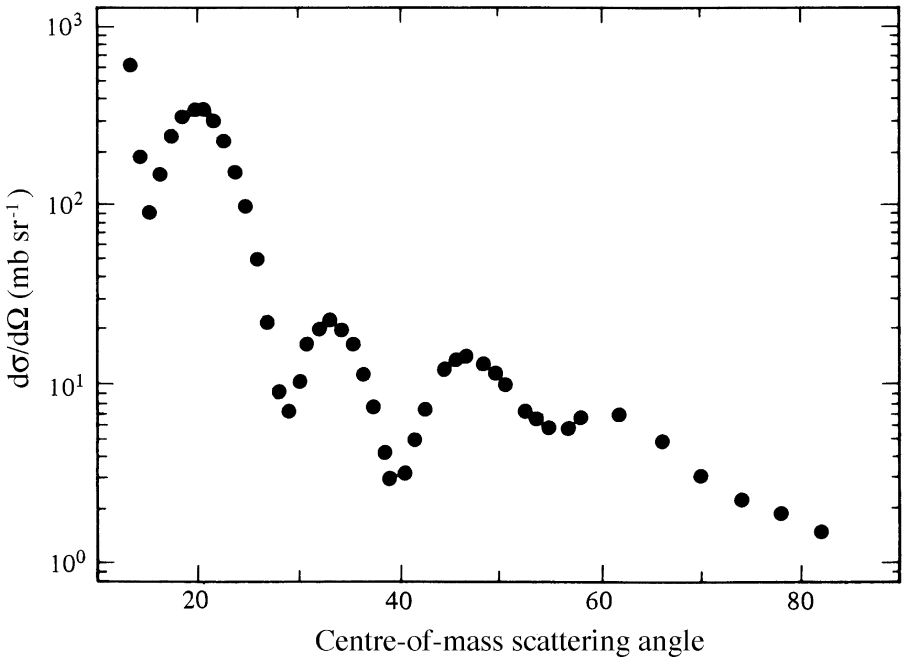

Figure 2.5 Elastic differential cross-sections for 52 MeV deuterons on ^{54}Fe (adapted from Hi68, copyright Elsevier, with permission)

nuclear case the imaginary part of a complex potential describing the interaction takes account of all the inelastic reactions. It is an essential feature of the model that the properties of nuclei are mainly determined by their size, as this implies that the same potential can account for the interaction of particles of different energies with different nuclei. Apart from the theoretical basis provided by analogy with classical optics, the model is essentially phenomenological, in that the values of the parameters of the optical potentials are found by optimizing the fit to the experimental data. This type of semi-phenomenological approach is common in both nuclear and particle physics.

In practice, the Schrödinger equation is solved using a parameterized complex potential where the real part is a sum of the Coulomb potential (for charged projectiles), an attractive nuclear potential and a spin-orbit potential, and the imaginary part is assumed to cause the incoming wave of the projectile to be attenuated within the nucleus, thereby allowing for inelastic effects. Originally, mathematical forms like Equation (2.23) were used to parameterize the real and imaginary parts of the potential, but subsequent work indicated substantial differences between the form factors of the real and imaginary parts of the potential and so different forms are now used for the imaginary part. The free parameters of the total potential are adjusted to fit the data.

The optical model has achieved its greatest success in the scattering of nucleons, but analyses using data obtained from light nuclei targets are also possible. A wide range of scattering data can be accounted for to a high degree of precision by

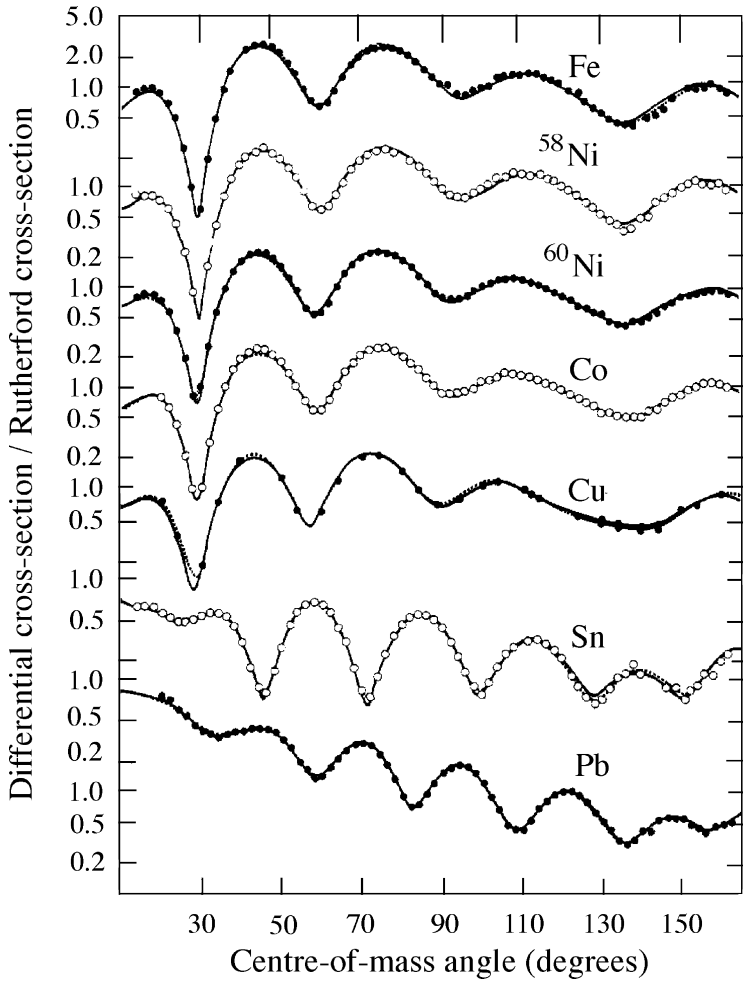

Figure 2.6 Differential cross-sections (normalized to the Rutherford cross-section) for the elastic scattering of 30.3 MeV protons, for a range of nuclei compared with optical model calculations; the solid and dashed lines represent the results using two different potentials (adapted from Sa67, copyright Elsevier, with permission)

the model and examples of this are shown in Figure 2.6. The corresponding wavefunctions are extensively used to extract information on nuclear structure. The conclusions are in accord with those above deduced indirectly from electron data.

2.3 Nuclear Instability

Stable nuclei only occur in a very narrow band in the $Z-N$ plane close to the line $Z = N$ (see Figure 2.7). All other nuclei are unstable and decay spontaneously in various ways. Isobars with a large surplus of neutrons gain energy by converting a

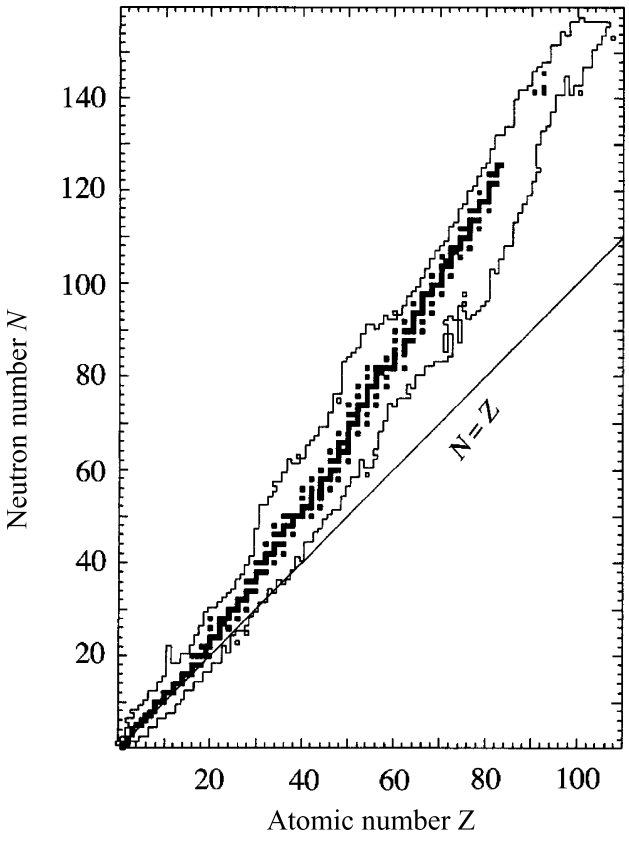

Figure 2.7 The distribution of stable nuclei: the squares are the stable and long-lived nuclei occurring in nature; other known nuclei lie within the jagged lines and are unstable. [adapted from Ch97.)

neutron into a proton; conversely, a nucleus with a large surplus of protons converts protons to neutrons. These are examples of β-decays, already mentioned. A related process is where an atomic electron is captured by the nucleus and a proton is thereby converted to a neutron within the nucleus. This is *electron capture* and like β-decay is a weak interaction. The electron is usually captured from the innermost shell and the process competes with β-decay in heavy nuclei because the radius of this shell (the K-shell) is close to the nuclei radius. The presence of a third particle in the decay process, the neutrino (as first suggested by Fermi), means that the emitted electrons (or positrons) have a continuous energy spectrum. The derivation and analysis of the electron momentum spectrum will be considered in Chapter 7 when we discuss the theory of β-decay.

The maximum of the curve of binding energy per nucleon is at approximately the position of iron (Fe) and nickel (Ni), which are therefore the most stable nuclides. In heavier nuclei, the binding energy is smaller because of the larger Coulomb repulsion. For still heavier nuclear masses, nuclei can decay spontaneously into two or more lighter nuclei, provided the mass of the parent nucleus is larger than the sum of the masses of the daughter nuclei.

Most such nuclei decay via two-body decays and the commonest case is when one of the daughter nuclei is a ^{4}He nucleus (i.e. an α-particle: $^4\mathrm{He} \equiv 2p2n$, with $A = 4\,,\ Z = N = 2$). The α-particle is favoured in such decays because it is a very stable, tightly bound structure. Because this is a two-body decay, the α-particle has a unique energy and the total energy released, the so-called *Q-value*, is given by:

$$Q_\alpha = (M_\mathrm{P} - M_\mathrm{D} - M_\alpha)c^2 = E_\mathrm{D} + E_\alpha, \tag{2.36}$$

where the subscripts refer to parent and daughter nuclei and the α-particle, and E is a kinetic energy.

The term *fission* is used to describe the rare cases where the two daughters have similar masses. If the decay occurs without external action, it is called *spontaneous fission* to distinguish it from *induced fission*, where some external stimulus is required to initiate the decay. Spontaneous fission only occurs with a probability greater than that for α-emission for nuclei with $Z \geq 110$. The reason for this is discussed in Section 2.7.

Finally, nuclei may decay by the emission of photons, with energies in the γ-ray part of the electromagnetic spectrum (*gamma emission*). This occurs when an excited nuclear state decays to a lower state and is a common way whereby excited states lose energy. The lower energy state is often the ground state. A competing process is *internal conversion*, where the nucleus de-excites by ejecting an electron from a low-lying atomic orbit. Both are electromagnetic processes. Electromagnetic decays will be discussed in more detail in Chapter 7.

2.4 Radioactive Decay

Before looking in more detail at different classes of instability, we will consider the general formalism describing the rate of radioactive decay. The probability per unit time that a given nucleus will decay is called its *decay constant* λ and is related to the *activity* $\mathscr{A}$ *by*

$$\mathscr{A} = -\mathrm{d}N/\mathrm{d}t = \lambda N, \tag{2.37}$$

where $N(t)$ is the number of radioactive nuclei in the sample at time t. The activity is measured in becquerels (Bq), which is one decay per second.[8] The probability here refers to the total probability, because λ could be the sum of decay probabilities for a number of distinct final states in the same way that the total decay width of an unstable particle is the sum of its partial widths. Integrating Equation (2.37) gives

$$\mathscr{A}(t) = \lambda N_0 \exp(-\lambda t), \tag{2.38}$$

where N_0 is the initial number of nuclei, i.e. the number at $t = 0$.

[8] An older unit, the curie ($1\ \mathrm{Ci} = 3.7 \times 10^{10}$ Bq) is also still in common use. A typical laboratory radioactive source has an activity of a few tens of kBq, i.e. μCi.

The *mean lifetime* τ of an unstable state, such as a radioactive nucleus or a hadron, follows from the general definition of a mean $\bar{x}$ of a distribution $f(x)$:

$$\bar{x} \equiv \left[\int x f(x)\,\mathrm{d}x\right] \Big/ \left[\int f(x)\,\mathrm{d}x\right]. \tag{2.39}$$

Thus

$$\tau \equiv \frac{\int t\,\mathrm{d}N(t)}{\int \mathrm{d}N(t)} = \frac{\int_0^\infty t\,\exp[-\lambda t]\,\mathrm{d}t}{\int_0^\infty \exp[-\lambda t]\,\mathrm{d}t} = \frac{1}{\lambda}. \tag{2.40}$$

This is the quantity we simply called 'the lifetime' in Chapter 1. The mean lifetime is always used in particle physics, but another measure more commonly used in nuclear physics is the *half-life* $t_{\frac{1}{2}}$, defined as the time for the number of nuclei to fall by one half. Thus $t_{\frac{1}{2}} = \ln 2/\lambda = \tau \ln 2$. In this book, the term *lifetime* will be used for the mean lifetime, both for radioactive nuclei and unstable hadrons, unless explicitly stated otherwise.

A well-known use of the radioactive decay law is in dating ancient specimens using the known properties of radioactive nuclei. For organic specimens, carbon is usually used. Carbon-14 is a radioactive isotope of carbon that is produced by the action of cosmic rays on nitrogen in the atmosphere.[9] If the flux of cosmic rays remains roughly constant over time, then the ratio of ^{14}C to the stable most abundant isotope ^{12}C reaches an equilibrium value of about $1:10^{12}$. Both isotopes will be taken up by living organisms in this ratio, but when the organism dies there is no further interaction with the environment and the ratio slowly changes with time as the ^{14}C nuclei decay by β-decay to ^{14}N with a lifetime of 8.27×10^3 years. Thus, if the ratio of ^{14}C to ^{12}C is measured, the age of the specimen may be estimated.[10] The actual measurements can be made very accurately because modern mass spectrometers can directly measure very small differences in the concentrations of ^{14}C and ^{12}C using only milligrams of material. Nevertheless, in practice, corrections are made to agree with independent calibrations if possible, using, for example, tree-ring growth data, because cosmic ray activity is not strictly constant with time.

In many cases the products of radioactive decay are themselves radioactive and so a decay chain results. Consider a decay chain $A \to B \to C \to \cdots$, with decay constants $\lambda_A,\ \lambda_B,\ \lambda_C$ etc.. The variation of species A with time is given by Equation (2.38), i.e.

$$N_A(t) = N_A(0)\exp(-\lambda_A t), \tag{2.41}$$

[9]Cosmic rays are high-energy particles, mainly protons, that impinge on the Earth's atmosphere from space. The products of the secondary reactions they produce may be detected at the Earth's surface. Victor Hess shared the 1936 Nobel Prize in Physics for the discovery of cosmic radiation.

[10]This method of using radioactive carbon to date ancient objects was devised by Willard Libby, for which he received the 1960 Nobel Prize in Chemistry.

but the differential equation for $N_B(t)$ will have an extra term in it to take account of the production of species B from the decay of species A:

$$\mathrm{d}N_B(t)/\mathrm{d}t = -\lambda_B N_B + \lambda_A N_A. \tag{2.42}$$

The solution of this equation may be verified by substitution to be

$$N_B(t) = \frac{\lambda_A}{\lambda_B - \lambda_A} N_A(0)[\exp(-\lambda_A t) - \exp(-\lambda_B t)]. \tag{2.43}$$

Similar equations may be found for decay sequences with more than two stages. Thus, for a three-stage sequence

$$N_C(t) = \lambda_A \lambda_B N_A(0) \left[\frac{\exp(-\lambda_A t)}{(\lambda_B - \lambda_A)(\lambda_C - \lambda_A)} + \frac{\exp(-\lambda_B t)}{(\lambda_A - \lambda_B)(\lambda_C - \lambda_B)} + \frac{\exp(-\lambda_C t)}{(\lambda_A - \lambda_C)(\lambda_B - \lambda_C)} \right] \tag{2.44}$$

As an example, the variation of the components as a function of time is shown in Figure 2.8 for the specific case:

$$\begin{aligned} {}^{79}_{38}\mathrm{Sr} &\rightarrow {}^{79}_{37}\mathrm{Rb} + e^+ + \nu_e \qquad (2.25\ \mathrm{min}) \\ &\hookrightarrow {}^{79}_{36}\mathrm{Kr} + e^+ + \nu_e \qquad (22.9\ \mathrm{min}) \\ &\hookrightarrow {}^{79}_{35}\mathrm{Br} + e^+ + \nu_e \qquad (35.04\ \mathrm{hours}) \end{aligned} \tag{2.45}$$

where the final nucleus is stable.

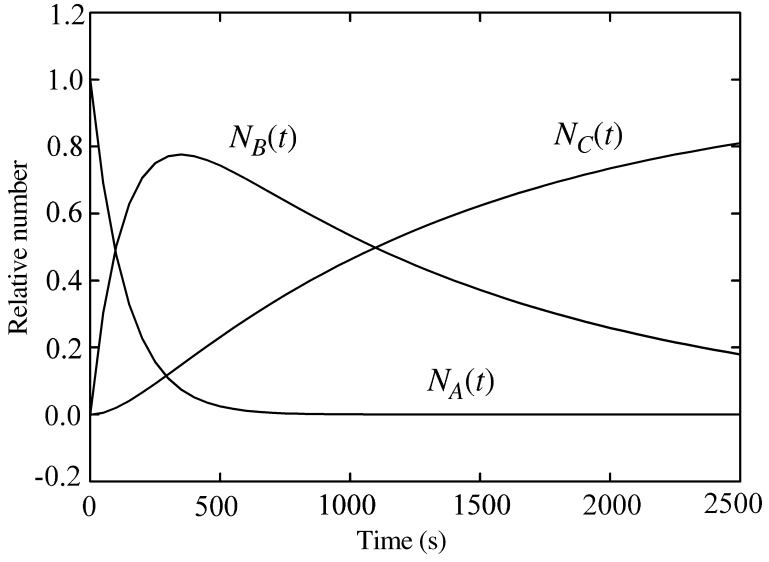

Figure 2.8 Time variation of the relative numbers of nuclei in the decay chain (2.45)

This illustrates the general features that whereas $N_A(t)$ for the initial species falls monotonically with time and $N_C(t)$ for the final stable species rises monotonically, $N_B(t)$ for an intermediate species rises to a maximum before falling. Note that at any time the sum of the components is a constant, as expected.

In the following sections we consider the phenomenology of the various types of radioactivity in more detail and in Chapter 7 we will return to discuss various models and theories that provide an understanding of these phenomena.

2.5 Semi-Empirical Mass Formula: The Liquid Drop Model

Apart from the lightest elements and a few special isolated very stable nuclei, the binding energy data of Figure 2.2 can be fitted by a simple formula containing just a few free parameters. This is the *semi-empirical mass formula* (SEMF), first written down in 1935 by Weizsäcker. It is a *semi*-empirical formula, because although it contains a number of constants that have to be found by fitting experimental data, the formula does have a theoretical basis. This arises from the two properties common to all nuclei (except those with very small A values) that we have seen earlier: (1) the interior mass densities are approximately equal, and (2) their total binding energies are approximately proportional to their masses. There is an analogy here with a classical model of a liquid drop, where for drops of various sizes: (1) interior densities are the same, and (2) latent heats of vaporization are proportional to their masses.[11] However, the analogy of a nucleus as an incompressible liquid droplet, with the nucleons playing the role of individual molecules within the droplet, cannot be taken too far because nucleons of course obey the laws of quantum, not classical, physics.

The semi-empirical mass formula will be taken to apply to *atomic* masses, as these are the masses actually observed in experiment. The atomic mass $M(Z, A)$ may then be written as the sum of six terms $f_i(Z,A)$:

$$M(Z, A) = \sum_{i=0}^{5} f_i(Z, A). \tag{2.46}$$

The first of these is the *mass of the constituent nucleons and electrons*,

$$f_0(Z, A) = Z\,(M_p + m_e) + (A - Z)M_n. \tag{2.47}$$

The remaining terms are various corrections, which we will write in the form a_i multiplied by a function of Z and A with $a_i > 0$.

The most important correction is the *volume* term,

$$f_1(Z, A) = -a_1 A. \tag{2.48}$$

[11] Latent heat is the average energy required to disperse the liquid drop into a gas and so is analogous to the binding energy per nucleon.

This arises from the fact that the strong nuclear force is short-range and each nucleon therefore feels the effect of only the nucleons immediately surrounding it (the force is said to be *saturated*), independent of the size of the nucleus. Recalling the important result deduced in Section 2.2 that the nuclear radius is proportional to $A^{\frac{1}{3}}$, this leads immediately to the binding energy being proportional to the volume, or nuclear mass. The coefficient is negative, i.e. it increases the binding energy, as expected.

The volume term overestimates the effect of the nuclear force because nucleons at the surface are not surrounded by other nucleons. Thus the volume term has to be corrected. This is done by the *surface* term

$$f_2(Z, A) = +a_2 A^{\frac{2}{3}}, \tag{2.49}$$

which is proportional to the surface area and decreases the binding energy. In the classical model of a real liquid drop, this term would correspond to the surface tension energy.

The *Coulomb* term accounts for the Coulomb energy of the charged nucleus, i.e. the fact that the protons repel each other. If we have a uniform charge distribution of radius proportional to $A^{\frac{1}{3}}$, then this term is

$$f_3(Z, A) = +a_3 \frac{Z(Z-1)}{A^{\frac{1}{3}}} \approx +a_3 \frac{Z^2}{A^{\frac{1}{3}}}, \tag{2.50}$$

where the approximation is sufficiently accurate for the large values of Z we will be considering. A similar effect would be present for a charged drop of a classical liquid.

The next term is the *asymmetry* term.

$$f_4(Z, A) = +a_4 \frac{(Z - A/2)^2}{A}. \tag{2.51}$$

This accounts for the observed tendency for nuclei to have $Z = N$. (There are no stable nuclei with very large neutron or proton excesses – c.f. Figure 2.7.) This term is purely quantum mechanical in origin and is due to the Pauli principle.

Part of the reason for the form (2.51) can be seen from the diagram of Figure 2.9, which shows the energy levels of a nucleus near the highest filled level in the approximation where all the energy levels are separated by the same energy Δ. Keeping A fixed and removing a proton from level 3 and adding a neutron to level 4, gives $(N - Z) = 2$ and leads to an energy increase of Δ. Repeating this for more protons, we find that the transfer of $(N - Z)/2$ nucleons decreases the binding energy by an amount $-\Delta(N - Z)^2/4$. Although we have assumed Δ is a constant, in practice it decreases like A^{-1}; hence the final form of the asymmetry term.

If we start with an even number of nucleons and progressively fill states, then the lowest energy will be when both Z and N are even. If, on the other hand, we have a

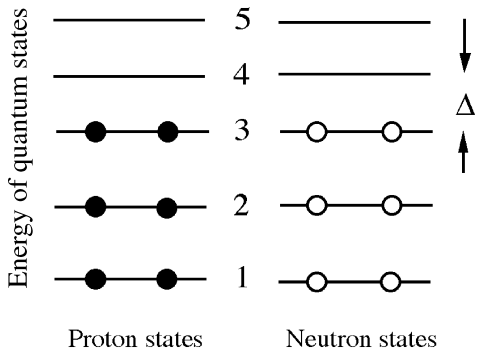

Figure 2.9 Schematic diagram of nuclear energy levels near the highest filled levels

system where both Z and N are odd and the highest filled proton state is above the highest filled neutron state, we can increase the binding energy by removing one proton from the nucleus and adding one neutron. If the highest filled proton state is below the highest filled neutron state, then we can produce the same effect by removing a neutron and adding a proton. These observations are summarized in the empirical *pairing* term, which maximizes the binding when both Z and N are even:

$$\begin{aligned} f_5(Z,A) &= -f(A), && \text{if } Z \text{ even}, A-Z=N \text{ even} \\ f_5(Z,A) &= 0, && \text{if } Z \text{ even}, A-Z=N \text{ odd; or, } Z \text{ odd}, A-Z=N \text{ even} \\ f_5(Z,A) &= +f(A), && \text{if } Z \text{ odd}, \ A-Z=N \text{ odd} \end{aligned} \tag{2.52}$$

The exact form of the function $f(A)$ is found by fitting the data; $f(A) = a_5 A^{-\frac{1}{2}}$ is often used.

To help remember these terms, the notation VSCAP is frequently used, with

$$a_1 = a_\mathrm{v}, \quad a_2 = a_\mathrm{s}, \quad a_3 = a_\mathrm{c}, \quad a_4 = a_\mathrm{a}, \quad a_5 = a_\mathrm{p}. \tag{2.53}$$

Precise values of the coefficients depend on the range of A fitted. One commonly used set is, in units of $\mathrm{MeV}/\mathrm{c}^2$:[12]

$$a_\mathrm{v} = 15.56, \quad a_\mathrm{s} = 17.23, \quad a_\mathrm{c} = 0.697, \quad a_\mathrm{a} = 93.14, \quad a_\mathrm{p} = 12. \tag{2.54}$$

The fit to the binding energy data for $A > 20$ using these coefficients in the SEMF is shown in Figure 2.10. Overall the fit to the data is remarkably good for such a simple formula, but is not exact of course. For example, there are a small number of regions where the binding energy curves show enhancements that are not reproduced. (These enhancements are due to the existence of a 'shell structure' of nucleons within the nucleus and will be discussed in Chapter 7.) Nevertheless, the SEMF gives accurate values for the binding energies for some 200 stable and many

[12]Note that some authors write the asymmetry term proportional to $(Z-N)^2$, which is equivalent to the form used here, but their value for the coefficient a_a will differ by a factor of four from the one in Equations (2.54).

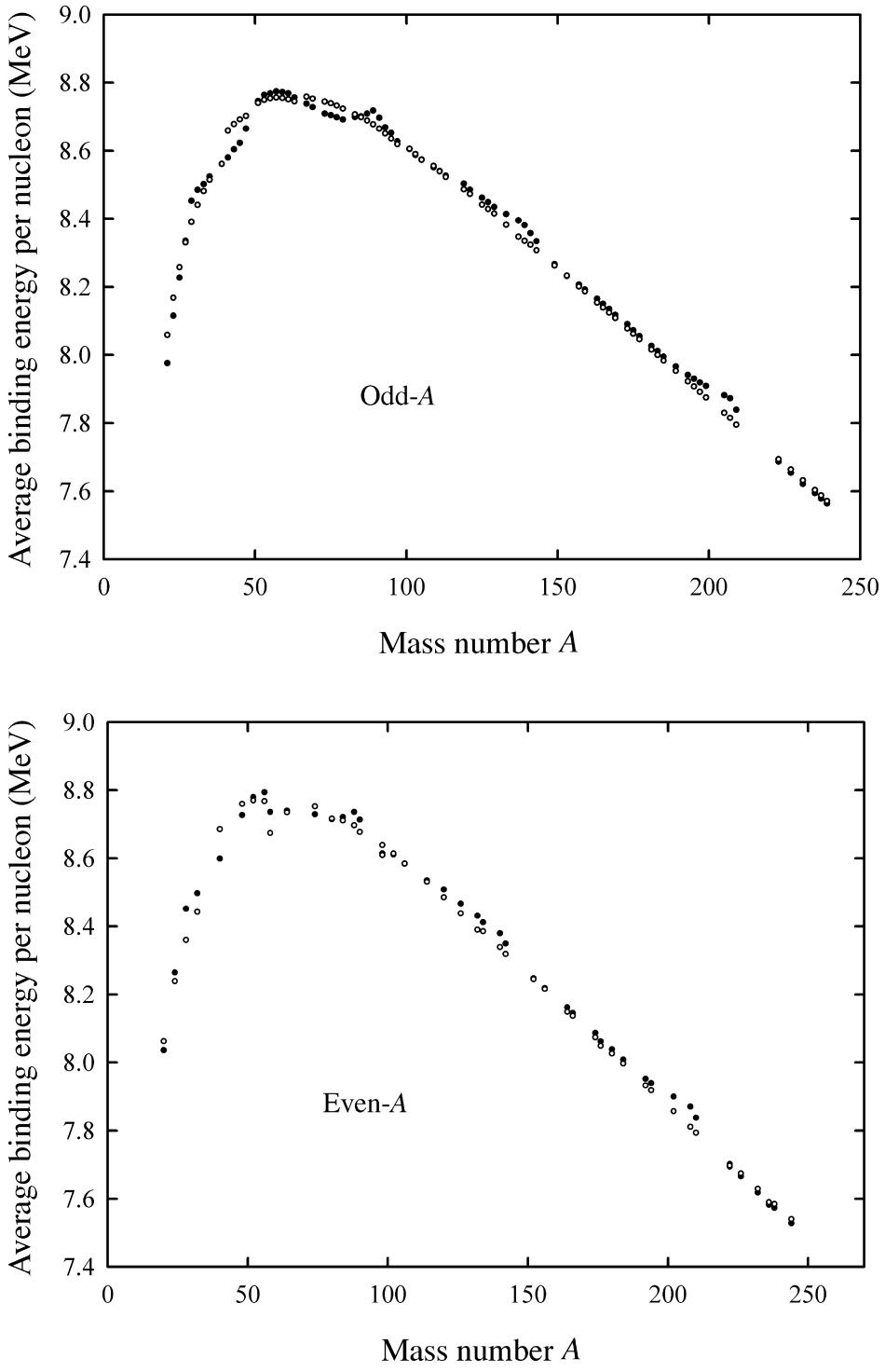

Figure 2.10 Fit to binding energy data (shown as solid circles) for odd-A and even-A nuclei using the SEMF with the coefficients given in the text; the predictions are shown as open circles and do not lie on smooth curves because A is not a function of Z

more unstable nuclei. We will use it to analyse the stability of nuclei with respect to β-decay and fission. The discussion of α-decay is deferred until Chapter 7.

Using the numerical values of Equation (2.54), the relative sizes of each of the terms in the SEMF may be calculated and for the case of odd-A are shown in Figure 2.11. In this diagram, the volume term is shown as positive and the other terms are subtracted from it to give the final SEMF curve.

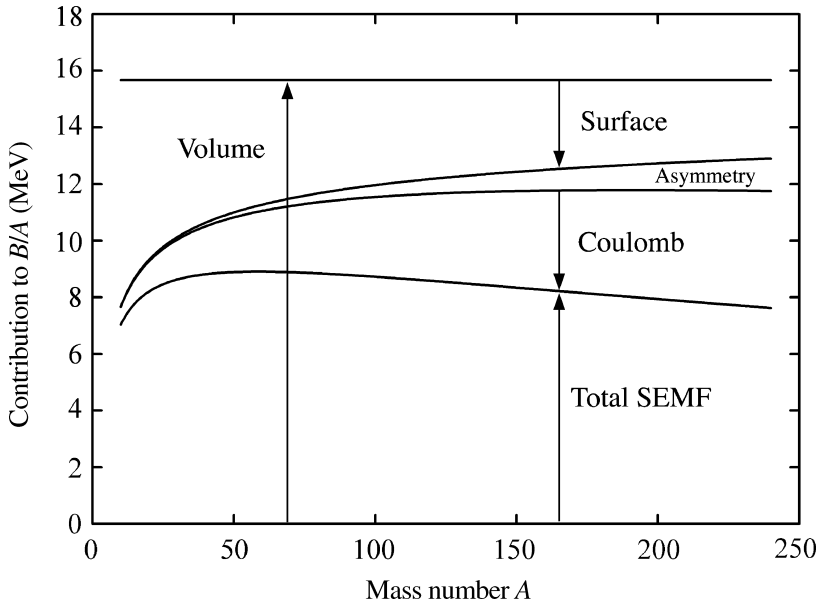

Figure 2.11 Contributions to the binding energy per nucleon as a function of mass number for odd-A from each term in the SEMF; the surface, asymmetry and Coulomb terms have been plotted so that they subtract from the volume term to give the total SEMF result in the lowest curve

Finally, from its definition, one might expect the binding energy per nucleon to be equivalent to the energy needed to remove a nucleon from the nucleus. However, to remove a neutron from a nucleus corresponds to the process

$$ {}^{A}_{Z}\mathrm{Y} \rightarrow {}^{A-1}_{Z}\mathrm{Y} + n \tag{2.55a} $$

and requires an energy change

$$ E_n = [M(Z,A-1) + M_n - M(Z,A)]c^2 = B(Z,A) - B(Z,A-1), \tag{2.55b} $$

whereas the removal of a proton corresponds to the process

$$ {}^{A}_{Z}\mathrm{Y} \rightarrow {}^{A-1}_{Z-1}\mathrm{X} + p, \tag{2.56a} $$

where X is a different chemical species to Y, and requires an energy change

$$E_p = \left[M(Z-1,A-1) + M_p + m_e - M(Z,A)\right]c^2 = B(Z,A) - B(Z-1,A-1) + m_e c^2. \tag{2.56b}$$

Thus, E_p and E_n are only equal to the binding energy per nucleon in an average sense. In practice, measurements show that E_p and E_n can differ substantially from this average and from each other at certain values of (Z, A). We will see in Chapter 7 that one reason for this is the existence of a shell structure for nucleons within nuclei, similar to the shell structure of electrons in atoms, which is ignored in the liquid drop model.

2.6 β-Decay Phenomenology

By rearranging terms, the SEMF (2.46) may be written

$$M(Z, A) = \alpha A - \beta Z + \gamma Z^2 + \frac{\delta}{A^{\frac{1}{2}}}, \tag{2.57}$$

where

$$\begin{aligned} \alpha &= M_n - a_v + \frac{a_s}{A^{\frac{1}{3}}} + \frac{a_a}{4} \\ \beta &= a_a + (M_n - M_p - m_e) \\ \gamma &= \frac{a_a}{A} + \frac{a_c}{A^{\frac{1}{3}}} \\ \delta &= a_p \end{aligned} \tag{2.58}$$

$M(Z,A)$ is thus a quadratic in Z at fixed A and has a minimum at $Z = \beta/2\gamma$. For a fixed value of A, a stable nucleus will have an integer value of Z closest to the solution of this equation. For odd A, the SEMF is a single parabola, but for even A the even–even and odd–odd nuclei lie on two distinct vertically shifted parabolas, because of the pairing term. The nucleus with the smallest mass in an isobaric spectrum is stable with respect to β-decay. We will consider the two cases of odd and even A separately, using specific values of A to illustrate the main features.

2.6.1 Odd-mass nuclei

Odd-mass nuclei can arise from even-N, odd-Z, or even-Z, odd-N configurations and in practice the number of nuclei that are stable against β-decay are roughly equally distributed between these two types. The example we take is the case of

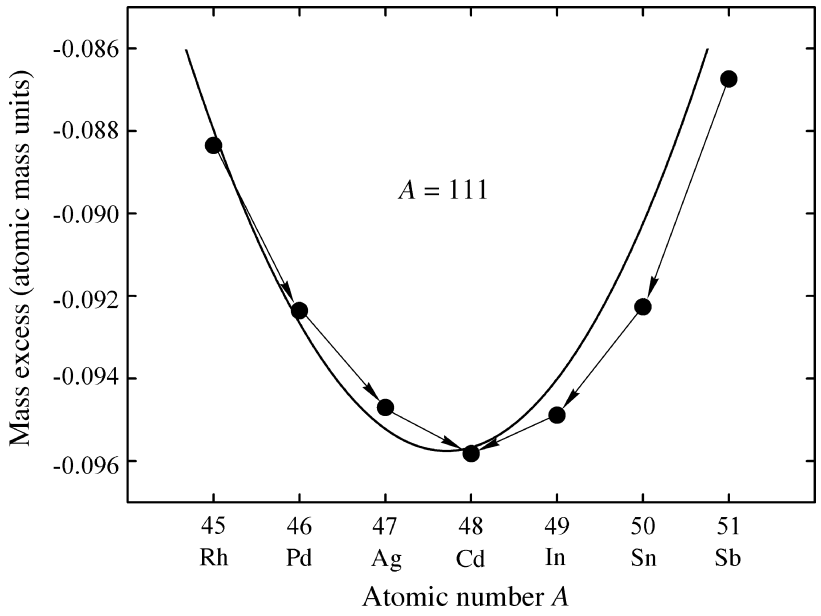

Figure 2.12 Mass parabola of the $A = 111$ isobars: the circles are experimental data and the curve is the prediction of the SEMF -- possible β-decays are indicated by arrows

the $A = 111$ isobars, which are shown in Figure 2.12. The circles show the experimental data as *mass excess* values in atomic mass units, where

$$\text{mass excess} \equiv M(Z,A)\ (\text{in atomic mass units}) - A \tag{2.59}$$

and the *atomic mass unit* (u) is defined as one twelfth of the mass of the neutral atom ${}^{12}_{6}\text{C}$.

The curve is the theoretical prediction from the SEMF using the numerical values of the coefficients (2.54). The exact form of the curve depends on the precise values of these coefficients. The minimum of the parabola corresponds to the isobar ${}^{111}_{48}\text{Cd}$ with $Z = 48$.

Isobars with more neutrons, such as ${}^{111}_{45}\text{Rh}$, ${}^{111}_{46}\text{Pd}$ and ${}^{111}_{47}\text{Ag}$, decay by converting a neutron to a proton, i.e.

$$n \rightarrow p + e^- + \bar{\nu}_e, \tag{2.60}$$

so that

$${}^{111}_{45}\text{Rh} \rightarrow {}^{111}_{46}\text{Pd} + e^- + \bar{\nu}_e \qquad (11\,\text{s}), \tag{2.61a}$$

$${}^{111}_{46}\text{Pd} \rightarrow {}^{111}_{47}\text{Ag} + e^- + \bar{\nu}_e \qquad (22.3\,\text{min}) \tag{2.61b}$$

and

$${}^{111}_{47}\text{Ag} \rightarrow {}^{111}_{48}\text{Cd} + e^- + \bar{\nu}_e \qquad (7.45\,\text{days}) \tag{2.61c}$$

This decay sequence is shown in Figure 2.12. Electron emission is energetically possible whenever the mass of the daughter atom $M(Z+1,A)$ is smaller than its isobaric neighbour, i.e.

$$M(Z,A) > M(Z+1,A). \tag{2.62}$$

Recall that we are referring here to *atoms*, so that the rest mass of the created electron is automatically taken into account.

Isobars with proton excess decay via

$$p \rightarrow n + e^{+} + \nu_e, \tag{2.63}$$

i.e. positron emission, which although not possible for a free proton, *is* possible in a nucleus because of the binding energy. So for example, the nuclei ${}^{111}_{51}\mathrm{Sb}$, ${}^{111}_{50}\mathrm{Sn}$ and ${}^{111}_{49}\mathrm{In}$ could, in principle, decay by positron emission, which is energetically possible if

$$M(Z,A) > M(Z-1,A) + 2m_e; \tag{2.64}$$

this takes account of the creation of a positron and the existence of an excess of electrons in the parent atom.

It is also theoretically possible for this sequence of transitions to occur by *electron capture*. This mainly occurs in heavy nuclei, where the electron orbits are more compact. It is usually the electron in the innermost shell (i.e. the K-shell) that is captured. Capture of such an electron gives rise to a 'hole' and causes electrons from higher levels to cascade downwards and in so doing emit characteristic X-rays. Electron capture is energetically allowed if

$$M(Z,A) > M(Z-1,A) + \varepsilon, \tag{2.65}$$

where ε is the excitation energy of the atomic shell of the daughter nucleus. The process competes with positron emission and in practice for the nuclei above this is what happens. Thus, we have

$$e^{-} + {}^{111}_{51}\mathrm{Sb} \rightarrow {}^{111}_{50}\mathrm{Sn} + \nu_e \quad (75\,\mathrm{s}), \tag{2.66a}$$

$$e^{-} + {}^{111}_{50}\mathrm{Sn} \rightarrow {}^{111}_{49}\mathrm{In} + \nu_e \quad (35.3\,\mathrm{min}) \tag{2.66b}$$

and

$$e^{-} + {}^{111}_{49}\mathrm{In} \rightarrow {}^{111}_{48}\mathrm{Cd} + \nu_e \quad (2.8\,\mathrm{days}), \tag{2.66c}$$

which are manifestations of the primary reaction

$$e^{-} + p \rightarrow n + \nu_e. \tag{2.67}$$

So once again we arrive at the stable isobar.

2.6.2 Even-mass nuclei

Even-mass nuclei can arise from even-N, even-Z, or odd-Z, odd-N configurations, but for reasons that are explained below, nearly all even-mass nuclei that are stable against β-decay are of the even–even type, with only a handful of odd–odd types known. Consider as an example the case of $A = 102$ shown in Figure 2.13. (Recall that the plot is of mass excess, which is a very small fraction of the total mass.)

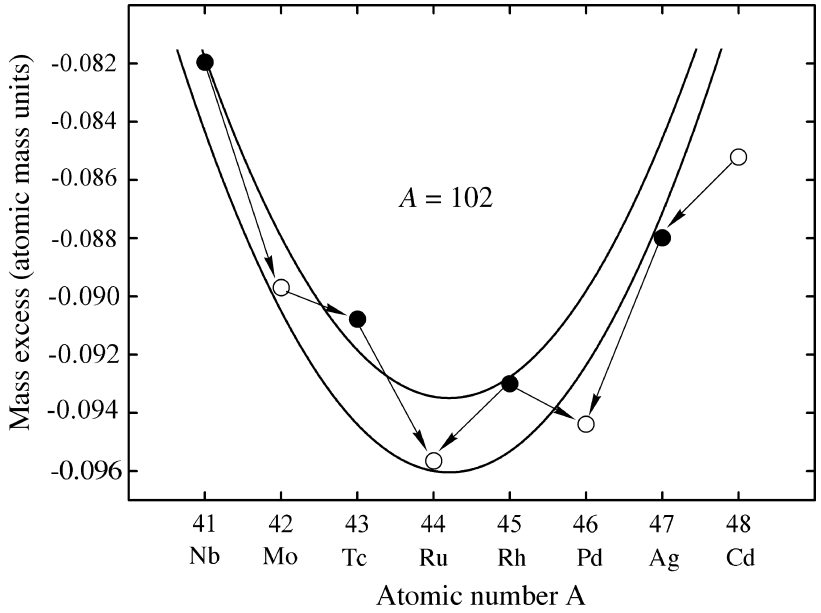

Figure 2.13 Mass parabolas of the $A = 102$ isobars: the circles are experimental data (open circles are even–even nuclei and closed circles are odd–odd nuclei); the curves are the prediction of the SEMF (upper curve is for odd--odd nuclei and lower curve for even–even nuclei) and possible β-decays are indicated by arrows

The lowest isobar is ${}^{102}_{44}\mathrm{Ru}$ and is β-stable. The isobar ${}^{102}_{46}\mathrm{Pd}$ is also stable since its two odd–odd neighbours both lie above it. In principle, the two nuclei could be connected by the reaction

$$ {}^{102}_{46}\mathrm{Pd} + 2e^- \rightarrow {}^{102}_{44}\mathrm{Ru} + 2\nu_e, \tag{2.68} $$

but this would involve a 'double electron capture' and would be heavily suppressed. The reaction has never been observed. Thus there are two β-stable isobars. This is a common situation for A-even, although no two neighbouring isobars are known to be stable. Odd–odd nuclei always have at least one more strongly bound even–even neighbour nucleus in the isobaric spectrum. They are therefore unstable. The only exceptions to this rule are a few very light nuclei.

The lifetime of a free neutron is about 887 s. The free proton is believed to be stable and can only 'decay' within a nucleus by utilizing the binding energy. Lifetimes of β emitters vary enormously from milliseconds to 10^{16} years. They

depend very sensitively on the Q-value for the decay and on the properties of the nuclei involved, e.g. their spins.

2.7 Fission

Spontaneous fission has been defined as the process whereby a parent nucleus breaks into two daughter nuclei of approximately equal masses without external action. Precisely equal masses are very unlikely and in the most probable cases the daughter nuclei have mass numbers that differ by about 45, with peaks around mass numbers 95 and 140. The reason for this is unknown. The binding energy curve shows that spontaneous fission is energetically possible for nuclei with $A > 100$.[13] An example is

$$^{238}_{92}\mathrm{U} \rightarrow {}^{145}_{57}\mathrm{La} + {}^{90}_{35}\mathrm{Br} + 3n, \tag{2.69}$$

with a release of about 154 MeV of energy, which is carried off as kinetic energy of the fission products. Heavy nuclei are neutron-rich and so necessarily produce neutron-rich decay products, including free neutrons. The fission products are themselves usually some way from the line of β-stability and will decay by a series of steps. For example, $^{145}_{57}$La decays to the β-stable $^{145}_{60}$Nd by three stages, releasing a further 8.5 MeV of energy, which in this case is carried off by the electrons and neutrinos emitted in β-decay. Although the probability of fission increases with increasing A, it is still a very rare process. For example, in $^{238}_{92}$U, the transition rate for spontaneous fission is about $3 \times 10^{-24}\,\mathrm{s}^{-1}$ compared with about $5 \times 10^{-18}\,\mathrm{s}^{-1}$ for α-decay, a branching fraction of 6×10^{-7}. Spontaneous emission only becomes dominant in very heavy elements with $A \geq 270$, as we shall now show.

To understand spontaneous fission we can again use the liquid drop model. In the SEMF we have assumed that the drop (i.e. the nucleus) is spherical, because this minimizes the surface area. However, if the surface is perturbed for some reason from spherical to prolate, the surface term in the SEMF will increase and the Coulomb term will decrease (assuming the volume remains the same) and the relative sizes of these two changes will determine whether the nucleus is stable against spontaneous fission.

For a fixed volume we can parametrize the deformation by the semi-major and semi-minor axes of the ellipsoid a and b, respectively as shown in Figure 2.14. One possible parametrization that preserves the volume is

$$a = R\,(1+\varepsilon), \quad b = R/(1+\varepsilon)^{\frac{1}{2}}, \tag{2.70}$$

where ε is a small parameter, so that

$$V = \frac{4}{3}\pi R^3 = \frac{4}{3}\pi ab^2. \tag{2.71}$$

[13]Fission in heavy nuclei was discovered by Otto Hahn, for which he received the 1944 Nobel Prize in Chemistry.

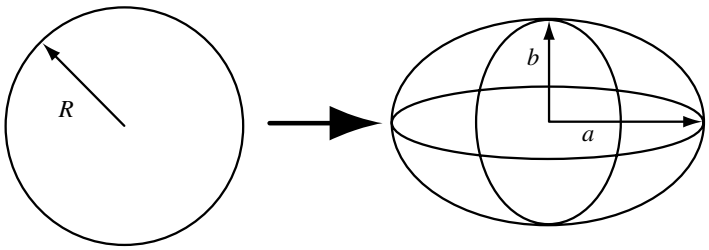

Figure 2.14 Deformation of a heavy nucleus

To find the new surface and Coulomb terms one has to find the expression for the surface of the ellipsoid in terms of a and b and expand it in a power series in ε. The algebra is unimportant and the results are:

$$E_s = a_s A^{\frac{2}{3}}\left(1 + \frac{2}{5}\varepsilon^2 + \ldots\right) \tag{2.72a}$$

and

$$E_c = a_c Z^2 A^{-\frac{1}{3}}\left(1 - \frac{1}{5}\varepsilon^2 + \ldots\right). \tag{2.72b}$$

Hence the change in the total energy is

$$\Delta E = (E_s + E_c) - (E_s + E_c)_{\text{SEMF}} = \frac{\varepsilon^2}{5}\left(2a_s A^{\frac{2}{3}} - a_c Z^2 A^{-\frac{1}{3}}\right). \tag{2.73}$$

If $\Delta E < 0$, then the deformation is energetically favourable and fission can occur. From Equation (2.73), this happens if

$$\frac{Z^2}{A} \geq \frac{2a_s}{a_c} \approx 49, \tag{2.74}$$

where we have used experimental values for the coefficients a_s and a_c given in Equations (2.54). The inequality is satisfied for nuclei with $Z > 116$ and $A \geq 270$.

Spontaneous fission is a potential barrier problem and this is shown in Figure 2.15. The solid line corresponds to the shape of the potential in the parent nucleus. The *activation energy* shown in Figure 2.15 determines the probability of spontaneous fission. To fission, the nucleus could in principle tunnel through the barrier, but the fragments are large and the probability for this to happen is extremely small.[14] For heavy nuclei the activation energy is about 6 MeV, but disappears for very heavy nuclei. For such nuclei, the shape of the potential corresponds closer to the dashed line and the slightest deformation will induce fission.

[14]The special case of α-decay will be discussed in Chapter 7. There we will show that the lifetime for such decays is expected to have an exponential dependence on the height of the fission barrier and this is observed qualitatively in fission data.

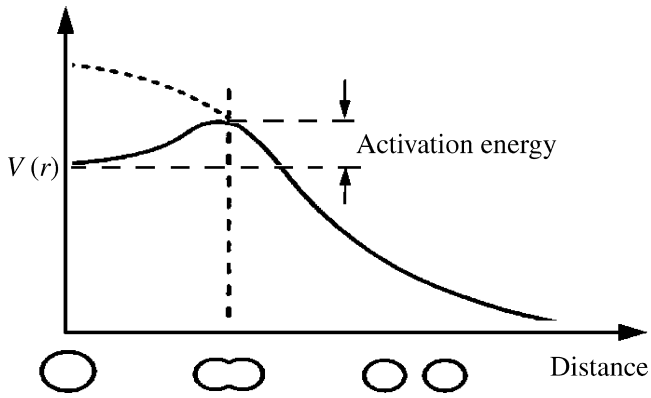

Figure 2.15 Potential energy during different stages of a fission reaction

Another possibility for fission is to supply the energy needed to overcome the barrier by a flow of neutrons. Because of the absence of a Coulomb force, a neutron can get very close to the nucleus and be captured by the strong nuclear attraction. The parent nucleus may then be excited to a state above the fission barrier and therefore split up. This process is an example of induced fission. Neutron capture by a nucleus with an odd neutron number releases not just some binding energy, but also a pairing energy. This small extra contribution makes a crucial difference to nuclear fission properties. For example, very low-energy ('thermal') neutrons can induce fission in ^{235}U, whereas only higher energy ('fast') neutrons induce fission in ^{238}U. This is because ^{235}U is an even–odd nucleus and ^{238}U is even–even. Therefore, the ground state of ^{235}U will lie higher (less tightly bound) in the potential well of its fragments than that of ^{238}U. Hence to induce fission, a smaller energy will be needed for ^{235}U than for ^{238}U. In principle, fission may be induced in ^{235}U using even zero-energy neutrons.[15]

We consider this quantitatively as follows. The capture of a neutron by ^{235}U changes an even–odd nucleus to a more tightly bound even–even (compound) nucleus of ^{236}U and releases the binding energy of the last neutron. In ^{235}U this is 6.5 MeV. As the activation energy (the energy needed to induce fission) is about 5 MeV for ^{236}U, neutron capture releases sufficient energy to fission the nucleus. The kinetic energy of the incident neutron is irrelevant and even zero-energy neutrons can induce fission in ^{235}U. In contrast, neutron capture in ^{238}U changes it from an even–even nucleus to an even–odd nucleus, i.e. changes a tightly bound nucleus to a less tightly bound one. The energy released (the binding energy of the last neutron) is about 4.8 MeV in ^{239}U and is less than the 6.5 MeV required for fission. For this reason, fast neutrons with energy of at least the difference between these two energies are required to fission ^{238}U.

[15]Enrico Fermi was a pioneer in the field of induced fission and received the 1938 Nobel Prize in Physics for 'demonstrations of the existence of new radioactive elements produced by neutron irradiation, and for his related discovery of nuclear reactions brought about by slow neutrons'. Fermi's citation could equally have been about his experimental discoveries and theoretical work in a wide range of areas from nuclear and particle physics to solid-state physics and astrophysics. He was probably the last 'universal physicist'.

2.8 γ-Decays

When a heavy nucleus disintegrates by either α- or β-decay, or by fission, the daughter nucleus is often left in an excited state. If this state is below the excitation energy for fission, it will de-excite, usually by emitting a high-energy photon. The energy of these photons is determined by the average energy level spacings in nuclei and ranges from a few to several MeV. They are in the gamma ray (γ) part of the electromagnetic spectrum. Because γ-decay is an electromagnetic process, we would expect the typical lifetime of an excited state to be $\sim 10^{-16}$ s. In practice, lifetimes are very sensitive to the amount of energy released in the decay and in the nuclear case other factors are also very important, particularly the quantity of angular momentum carried off by the photon. Typical lifetimes of nuclear levels are about $\sim 10^{-12}$ s.

The role of angular momentum in γ-decays is crucial. If the initial (excited) state has a total spin $\mathbf{S}_\mathrm{i}$ and the final nucleus has a total spin $\mathbf{S}_\mathrm{f}$, then the total angular momentum $\mathbf{J}$ of the emitted photon is given by

$$\mathbf{J} = \mathbf{S}_\mathrm{i} - \mathbf{S}_\mathrm{f}, \tag{2.75}$$

with

$$S_\mathrm{i} + S_\mathrm{f} \geq J \geq |S_\mathrm{i} - S_\mathrm{f}|, \tag{2.76}$$

where $S = |\mathbf{S}|,\ J = |\mathbf{J}|$. In addition,

$$m_\mathrm{i} = M + m_\mathrm{f}, \tag{2.77}$$

where m are the corresponding magnetic quantum numbers. Both total angular momentum and its magnetic quantum number are conserved in γ-decays.

γ-decays are further complicated because parity is conserved in these electromagnetic processes. Both the initial and final nuclear level will have an intrinsic parity, as does the photon, and in addition there is a parity associated with the angular momentum carried off by the photon, which is of the form $(-1)^J$, reflecting the symmetry of the angular part of the wavefunction (see Equation (1.14)). We will not pursue this further here, but defer a more detailed discussion until Chapter 7.

2.9 Nuclear Reactions

In Chapter 1 and earlier sections of the present chapter we discussed various aspects of reactions. In particle physics, because the projectiles and targets have relatively simple structures, this is all that is required in classifying reactions. In nuclear physics, however, because the target has a rich structure it is useful to classify reactions in more detail. In this section we do this, drawing together our previous work and also anticipating some reactions that will be encountered in later chapters.

Elastic scattering reactions were defined in Chapter 1 as those interactions where the initial and final particles are identical, i.e. $a + A \rightarrow a + A$. We also defined inelastic scattering as the situation where the final particles are the same chemical species, but one or more is in an excited state, e.g. $a + A \rightarrow a + A^*$ and in Section 2.1 we showed how the kinematics of such reactions could be used to determine the mass of the excited state. Elastic and inelastic scattering are examples of so-called *direct reactions*. These are defined as ones where the incident particle interacts in a time comparable to the time taken to transit the nucleus. They are more likely when the incident particle has an energy corresponding to a de Broglie wavelength closer to the size of a nucleon rather than that of the nucleus. The collisions are largely peripheral, with only a relatively small fraction of the available energy transferred to the target. Another direct reaction is $^{16}\mathrm{O}(p,d)^{15}\mathrm{O}$, i.e.

$$p + {}^{16}\mathrm{O} \rightarrow d + {}^{15}\mathrm{O}, \tag{2.78}$$

where we have used the notation $A(a,b)B$ for the general nuclear reaction $a + A \rightarrow b + B$. This is an example of a *pick-up reaction*, because one or more nucleons (in this case a neutron) is stripped off the target nucleus and carried away by the projectile. The 'inverse' of this reaction is $^{16}\mathrm{O}(d,p)^{17}\mathrm{O}$. This is an example of a *stripping reaction*, because one or more nucleons (in this case again a neutron) is stripped off the projectile and transferred to the target nucleus.

The theoretical interpretation of direct reactions is based on the assumption that the projectile experiences the average potential of the target nucleus. For example, we have seen in the optical model of Section 2.2.2 how this approach can be used to analyse differential cross sections for elastic scattering and be used to extract information about nuclear shapes and sizes. It also leads to the prediction of resonances of width typically of order 1 MeV separated by a few MeV, as observed in cross-section as functions of centre-of-mass energy for nucleon scattering from light nuclei. One way of viewing this is as a consequence of the reaction time for a direct reaction, typically 10^{-22} s , making use of the uncertainty relation between energy and time, $\Delta E \Delta t \geq \hbar$.

A second important class of interactions is where the projectile becomes loosely bound in the nucleus and shares its energy with all the nuclear constituents. This is called a *compound nucleus reaction*. The time for the system to reach statistical equilibrium depends on the nuclear species, the type of projectile and its energy, but will always be much longer than the transit time and is typically several orders of magnitude longer. An important feature of these reactions is that the properties of the compound nucleus determine its subsequent behaviour and not the mechanism by which it was formed. The compound nucleus is in an excited state and is inherently unstable. Eventually, by a statistical fluctuation, one or more nucleons will acquire sufficient energy to escape and the nucleus either emits particles or de-excites by radiating gamma rays.

If the compound nucleus is created in a region of excitation where its energy levels are well separated, the cross-section will exhibit well-defined resonances

described by the Breit–Wigner formula of Section 1.6.3. These processes are depicted schematically in the energy-level diagram of Figure 2.16, which correspond to $a + A \rightarrow C^* \rightarrow b + B$, where C^* is the compound nucleus and $a + A \rightarrow C^* \rightarrow C + \gamma$, where C is the ground state corresponding to the excited state C^*. In practice, there could be many final states to which C^* could decay.

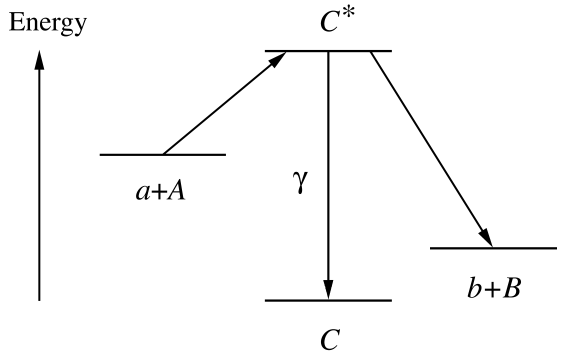

Figure 2.16 Energy-level diagram showing the excitation of a compound nucleus $C^*$and its subsequent decay

Because the time for a compound nucleus to reach statistical equilibrium is much longer than the transit time for a direct reaction, the cross-sections for a compound nucleus process can show variations on much smaller energy scales than those for direct reactions. The density of levels in the compound nucleus is high, and so a very small change in the incident energy suffices to alter completely the intermediate states, and hence the cross section. An example is shown in Figure 2.17, which gives the total cross-section for neutron scattering from ^{12}C at neutron laboratory energies of a few MeV. Peaks corresponding to resonance formation in ^{13}C are clearly identified. Their widths vary from a few tens to a few hundreds of keV, consistent with the characteristic times for compound nucleus formation and decay.

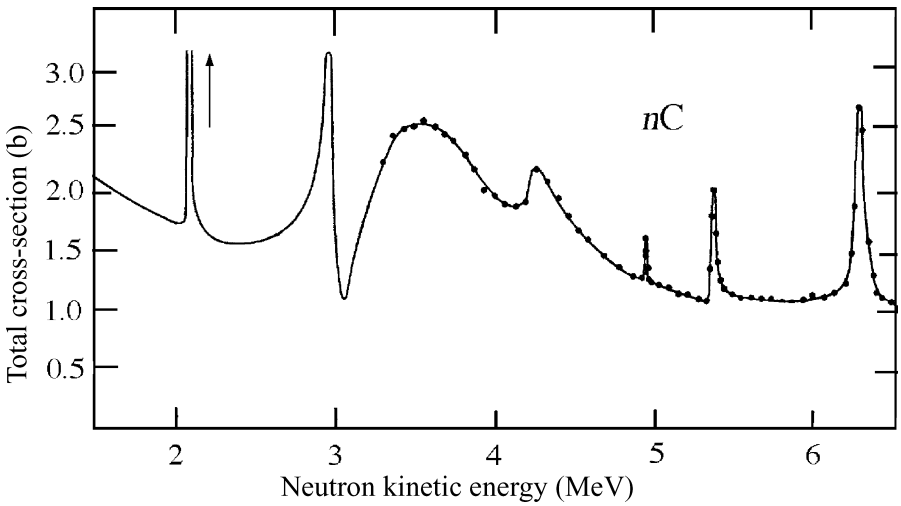

Figure 2.17 Total cross-section for n^{12}C interactions (adapted from Fo61. Copyright American Physical Society.)

The mean widths of compound nucleus excitations depend on the incident energy and the target nucleus, decreasing both with energy and rapidly with nuclear mass. Neutrons, because they are neutral, have a high probability of being captured by nuclei and their cross-sections are rich in compound nucleus effects, particularly at very low energies. This is discussed further below.

The division of reactions into direct and compound nucleus is not exhaustive and situations can occur where particles are ejected from the nucleus before full statistical equilibrium has been reached. Also, in the collisions of complex heavy ions, there is an appreciable probability for an additional reaction mechanism called *deep inelastic scattering* that is intermediate between direct and compound nucleus reactions. In this case, the probability for complete fusion of the colliding ions is small, but there can be substantial transfer of the incident kinetic energy to internal excitations of the ions. We will not discuss this or other mechanisms further, but we will encounter the concept of deep inelastic scattering again in Chapter 5 in the context of exploring the internal structure of nucleons. In practice, the various mechanisms feed the same final states as direct reactions. This is illustrated schematically in Figure 2.18 for reactions initiated using protons as the projectile.

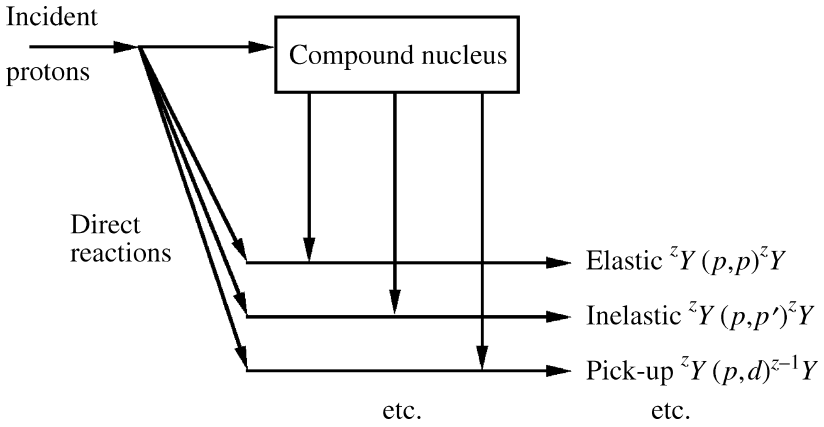

Figure 2.18 Direct and compound nucleus reactions in nuclear reactions initiated by protons

The general form of the yield $N(E)$ of secondary particles at a fixed angle as a function of the outgoing energy E, i.e. the number of particles with energy E between E and $E + \mathrm{d}E$, is shown schematically in Figure 2.19 for the case of an incident nucleon. At the upper end of the plot (which corresponds to low-incident nucleon energies) there are a number of distinct peaks due to elastic, inelastic and transfer reactions. Then as the excitation energy is reduced, the more closely-spaced energy levels in the final nucleus are not fully resolved because of the spread in energy of the incident beam and the uncertainty in the experimental measurements of energy. At the lowest energies there is a broad continuum mainly due to the decays of compound nuclei formed by the absorption of the projectile nucleon by the target nucleus. The differential cross-sections for the two processes will be very different. Direct reactions lead to a cross-section peaked in the forward direction, falling rapidly with angle and with oscillations, as we have seen

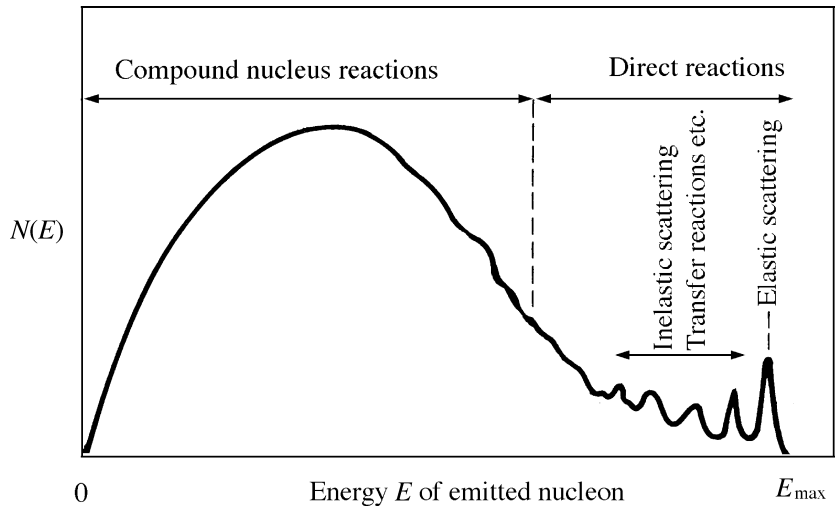

Figure 2.19 Typical spectrum of energies of the nucleons emitted at a fixed angle in inelastic nucleon--nucleus reactions

in the case of elastic scattering in Section 2.2 (Figure 2.3). On the other hand, the contribution from the compound nucleus at low energies where an isolated compound nucleus is formed is fairly isotropic and symmetric about 90°.

Many medium- and large-A nuclei can capture low-energy ($\sim$(10–100) eV) neutrons very readily. The neutron separation energy for the final nucleus is $\sim$6 MeV and thus capture leads to a compound nucleus with an excitation energy above the ground state by this separation energy. Such excitation often occurs in a region of high density of narrow states that show up as a rich resonance structure in the corresponding neutron total cross-section. An example is shown in Figure 2.20. The value of the cross-section at the resonance peaks can be many orders of

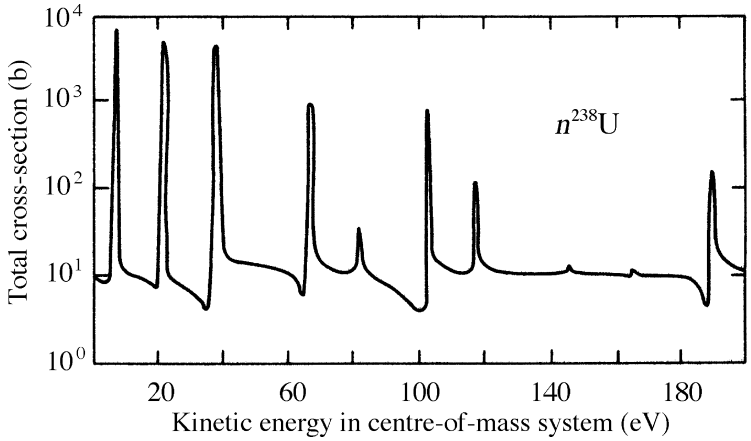

Figure 2.20 Total cross-section for neutron interactions with ^{238}U, showing many very narrow resonances (with intrinsic widths of order 10^{-2} eV) corresponding to excited states of ^{239}U (from Ga76, courtesy of Brookhaven National Laboratory)

magnitude greater than the geometrical cross-section based on the size of the nucleus. This is because the cross-section is determined dominantly by the area associated with the wavelength λ of the projectile, i.e. $\pi\lambda^2$, which is very large because λ is large.

Once formed, the compound nucleus can decay to any final state consistent with the relevant conservation laws. If this includes neutron emission, it will be the preferred decay. However, for production by very slow (thermal) neutrons with energies of the order of 0.02 eV, the available decay kinetic energy will reflect the initial energy of the projectile, which is very small. Therefore, in these cases, photon emission is often preferred. We shall see in Chapter 8 that the fact that radiative decay is the dominant mode of decay of compound nuclei formed by thermal neutrons is important in the use of nuclear fission to produce power in nuclear reactors.

Problems

2.1 Electrons with momentum 330 MeV/c are elastically scattered through an angle of 10° by a nucleus of ^{56}Fe. If the charge distribution on the nucleus is assumed to be that of a uniform hard sphere, and assuming the Born approximation is valid, by what factor would you expect the Mott cross-section to be reduced?

2.2 Show explicitly that Equation (2.28) follows from Equation (2.26).

2.3 A beam of electrons with energies 250 MeV is scattered through an angle of 10° by a heavy nucleus. It is found that the differential cross-section is 65 per cent of that expected from scattering from a point nucleus. Estimate the root mean square radius of the nucleus.

2.4 Find the form factor for a charge distribution $\rho(r) = \rho_0 \exp(-r/a)/r$, where ρ_0 and a are constants.

2.5 A sample of 1 g of a radioactive isotope of atomic weight 208 decays via β-emission and 75 counts are recorded in a 24 h period. If the detector efficiency is 10 per cent, estimate the mean life of the isotope.

2.6 A 1 g sample taken from an organic artefact is found to have a β count rate of 2.1 counts per min, which are assumed to originate from the decay of ^{14}C with a mean lifetime of 8270 years. If the abundance of ^{14}C in living matter is currently 1.2×10^{-12}, what can you deduce about the approximate age of the artefact?

2.7 Nuclei of $^{212}_{86}$Rn decay by α-emission to $^{208}_{84}$Po with a mean life of 23.9 min. The $^{208}_{84}$Po nuclei in turn decay, also by α-emission, to the stable isotope $^{204}_{82}$Pb with a mean life of 2.9 years. If initially the source is pure $^{212}_{86}$Rn, how long will it take for the rate of α-emission in the final decay to reach a maximum?

2.8 Natural lanthanum has an atomic weight of 138.91 and contains 0.09 per cent of the isotope $^{138}_{57}\mathrm{La}$. This has two decay modes: $^{138}_{57}\mathrm{La} \rightarrow {}^{138}_{58}\mathrm{Ce} + e^- + \bar{\nu}_e$ (β-decay) and $^{138}_{57}\mathrm{La} + e^- \rightarrow {}^{138}_{56}\mathrm{Ba}^* + \nu_e$ (electron capture), followed by the electromagnetic decay of the excited state $^{138}_{56}\mathrm{Ba}^* \rightarrow {}^{138}_{56}\mathrm{Ba} + \gamma$ (radiative decay). There are 7.8×10^2 β-particles emitted per s per kg of natural lanthanum and there are 50 photons emitted per 100 β-particles. Estimate the mean lifetime of $^{138}_{57}\mathrm{La}$.

2.9 Use the SEMF to estimate the energy released in the spontaneous fission reaction

$$^{235}_{92}\mathrm{U} \rightarrow {}^{87}_{35}\mathrm{Br} + {}^{145}_{57}\mathrm{La} + 3n.$$

2.10 The most stable nucleus with $A = 111$ is $^{111}_{48}\mathrm{Cd}$ (see Figure 2.12). By what percentage would the fine structure constant α have to change if the most stable nucleus with $A = 111$ were to be $^{111}_{47}\mathrm{Ag}$? Assume that altering α does not change particle masses.

2.11 The transuranic isotope $^{269}_{108}\mathrm{Hs}$ decays 100 per cent via α-emission with a lifetime of 27 s, i.e. $^{269}_{108}\mathrm{Hs} \rightarrow {}^{265}_{106}\mathrm{Sg} + \alpha$, where the kinetic energy of the α-particle is $E_\alpha = 9.23$ MeV. Calculate the mass of the $^{269}_{108}\mathrm{Hs}$ nucleus in atomic mass units.

2.12 The isotope $^{238}_{94}\mathrm{Pu}$ decays via α-emission to the essentially stable isotope $^{234}_{92}\mathrm{U}$ with a lifetime of 126.7 years and a release of 5.49 MeV of kinetic energy. This energy is converted to electrical power in a space probe designed to reach planet X in a journey planned to last 4 years. If the efficiency of power conversion is 5 per cent and on reaching planet X the probe requires at least 200 W of power to perform its landing tasks, how much $^{238}_{94}\mathrm{Pu}$ would be needed at launch?

2.13 On planet X it is found that the isotopes $^{205}\mathrm{Pb}(\tau = 1.53 \times 10^7\mathrm{y})$ and $^{204}\mathrm{Pb}$ (stable) are present with abundances n_{205} and n_{204}, with $n_{205}/n_{204} = 2 \times 10^{-7}$. If at the time of the formation of planet X both isotopes were present in equal amounts, how old is the planet?

2.14 The reaction $^{45}_{21}\mathrm{Sc}(d,p)^{46}_{21}\mathrm{Sc}$ has a Q-value of 6.54 MeV and a resonance when the incident deuteron laboratory kinetic energy is 2.76 MeV. Would you expect the same resonance to be excited in the reaction $^{43}_{20}\mathrm{Ca}(\alpha,n)^{46}_{22}\mathrm{Ti}$ and if so at what value of the laboratory kinetic energy of the alpha particle? You may use the fact that the β-decay $^{46}_{21}\mathrm{Sc} \rightarrow {}^{46}_{22}\mathrm{Ti} + e^- + \bar{\nu}_e$ has a Q-value of 2.37 MeV and the mass difference between the neutron and a hydrogen atom is 0.78 MeV/c^2.

2.15 A radioisotope with decay constant λ is produced at a constant rate P. Show that the number of atoms at time t is $N(t) = P[1 - \exp(-\lambda t)]/\lambda$.

2.16 Radioactive $^{36}\mathrm{Cl}$ (half-life 3×10^5 years) is produced by irradiating 1 g of natural nickel chloride ($NiCl_2$, molecular weight 129.6) in a neutron beam of flux $F = 10^{14}\mathrm{cm}^{-2}\mathrm{s}^{-1}$. If the neutron absorption cross-section $^{35}\mathrm{Cl}(n,\gamma)^{36}\mathrm{Cl}$ is $\sigma = 43.6$ b and 75.8 per cent of natural chlorine is $^{35}\mathrm{Cl}$, use the result of Problem 2.15 to estimate the time it would take to produce a 3×10^5 Bq source of $^{36}\mathrm{Cl}$.

2.17 Consider the total cross-section data for the n^{238}U interaction shown in Figure 2.20. There is a resonance R at the centre-of-mass neutron kinetic energy $E_n = 10$ eV with width $\Gamma = 10^{-2}$ eV and the total cross-section there is $\sigma_{\max} = 9 \times 10^3$ b. Use this information to find the partial widths $\Gamma_{n,\gamma}$ for the decays $R \rightarrow n + {}^{238}$U and $R \rightarrow \gamma + {}^{238}$U, if these are the only two significant decay modes. The spin of the ground state of ^{238}U is zero.